Chemical Engineering Journal Advances 9 (2022) 100187

Contents lists available at ScienceDirect

Chemical Engineering Journal Advances

journal homepage: www.sciencedirect.com/journal/chemical-engineering-journal-advances

Development of a novel, through-flow microwave-based regenerator for sorbent-based direct air capture

T.N. van Schagen *, P.J. van der Wal, D.W.F. Brilman *

Sustainable Process Technology, Faculty of Science and Technology, University of Twente, PO Box 217, Enschede 7500 AE, the Netherlands

ARTICLE INFO

Keywords:
Direct air capture
CO_2 adsorption
Sorbent regeneration
Microwave desorption
Lewatit VP OC 1065

ABSTRACT

In this work an all-electric regenerator is developed for the desorption of CO_2 from air-capture sorbents using microwaves. An electromagnetic model was made for a continuous flow radial desorber and its dimensions were optimised for maximal microwave utilisation. Based on the optimal dimensions an actual prototype, capable of desorbing CO_2 from a commercial supported amine sorbent in fixed- or moving-bed configuration was built to demonstrate the concept and to study performance characteristics. TSA experiments using nitrogen as purge gas to produce enriched air (1 to 2 vol.% CO_2) were done. Productivities of up to 1.5 kg $CO_2/kg_{sorb.}/d$ were demonstrated, with a total energy duty of 25 MJ/kg CO_2. Compared to traditional TVSA desorption, the energy duty is similar while the productivity is significantly higher. The process can be further improved by creating an even more homogeneous electric field (preventing hot spots in the regenerator) and by enabling desorption under vacuum conditions to produce pure CO_2. Overall, microwave desorption is demonstrated as an effective way to circumvent heat transfer limitations present during more traditional thermal desorption processes using polymeric sorbents.

1. Introduction

Since Lackner et al. proposed the capture of CO_2 directly from air as mitigation of climate change [1], a lot of work has been done in this field. With the ever-increasing global CO_2 emissions [2], air capture becomes increasingly more important to limit global temperature rise as outlined by the Intergovernmental Panel on Climate Change (IPCC) [3]. DAC technology is being developed rapidly, and already applied commercially to some degree by companies like Climeworks, Global Thermostat and Carbon Engineering. Different technologies are applied ranging from CO_2 absorption by alkaline solutions [4] or liquid amines [5], to adsorption techniques using a variety of sorbents [6,7]. Most work focuses on adsorption systems, using temperature and/or vacuum swing adsorption (TSA, VSA, TVSA) [7–10]. This is because solid, supported amine sorbents generally have favourable properties for air capture, like a high CO_2 equilibrium loading, relatively fast kinetics and reasonable stability [11,12].

Since adsorption is spontaneous and inherently exothermic, desorption is endothermic and thus energy must be supplied during this step. Usually this is done using thermal energy. However, the most commonly used sorbents (amine-functionalised porous polymeric particles) are relatively poor conductors making the supply of energy to the CO_2 sites on the sorbent a challenge [11,13,14]. Because of this, in many adsorption systems the desorption time is dictated by the heat transfer rate, which also limits the overall CO_2 productivity. Using a higher imposed desorption temperature could accelerate heat transfer, but in practice the desorption temperature is limited by the sorbent stability [12,15].

Alternative heating and desorption methods for CO_2 capture sorbents are therefore being researched. Examples are the use of phase-change materials [16], moisture-swing sorbents [17], steam desorption [18], induction heating of magnetised sorbents [19] and the use of Joule heating [20]. The mentioned alternative methods do have some drawbacks compared to traditional thermal desorption, including the need for special sorbent materials [17,19,20] and the dependence of the process on ambient humidity in the case of moisture-swing adsorption [17]. Furthermore, the poor thermal conductivity of the sorbent still limits desorption performance in some cases [16,18].

Another way to circumvent heat transfer limitations in sorbents is to use microwave heating. Microwave radiation can heat materials volumetrically via dielectric heating. While during conventional heating, the heat flux to a system is dictated by the specific surface area, heat transfer coefficient and applied temperature difference, during microwave

* Corresponding authors.
E-mail addresses: t.n.vanschagen@utwente.nl (T.N. van Schagen), wim.brilman@utwente.nl (D.W.F. Brilman).

https://doi.org/10.1016/j.ceja.2021.100187
Received 17 September 2021; Accepted 20 September 2021
Available online 3 October 2021

List of symbols

Symbol	Description	Unit
ϕ	relative humidity	(–)
q	sorbent loading	(mol kg^{-1})
C_m	GAB isotherm parameter	(mol kg^{-1})
C_G	GAB isotherm parameter	(–)
K_{ads}	GAB isotherm parameter	(–)
C_0	GAB isotherm parameter	(–)
$\Delta_c H$	GAB isotherm parameter	(J mol^{-1})
R	gas constant	(J mol^{-1} K^{-1})
T	temperature	(K)
K_0	GAB isotherm parameter	(–)
$\Delta_k H$	GAB isotherm parameter	(J mol^{-1})
P_d	power dissipation	(W m^{-3})
f	electromagnetic frequency	(Hz)
ε_0	vacuum dielectric permittivity	(F m^{-1})
ε'	real part of dielectric permittivity	(–)
ε''	complex part of dielectric permittivity (loss factor)	(–)
ν	volume fraction	(–)
$\tan\delta$	loss angle tangent	(–)
λ	wavelength	(m)
d	diameter	(m)
l	length	(m)
t	time	(m)
Q	duty	(W)
ϕ_V	volumetric flow rate	(m^3 s^{-1})
U	voltage	(V)
I	electric current	(A)
m	mass	(kg)
p	pressure	(Pa)
x	mole fraction	(–)
M_w	molar mass	(kg mol^{-1})
φ	phase angle	(–)
C_p	specific heat capacity	(J kg^{-1} K^{-1})
n	number of moles	(mol)
$\Delta_{ads}H$	heat of adsorption	(J mol^{-1})

regeneration the heat flux is almost independent of temperature and instead dictated by the overall geometry. The idea to use microwaves for the regeneration of sorbents was first proposed by Roussy and Chenot [21] in the context of water desorption from zeolite 13X. Cherbański and Molga [22] discusses various aspects of the use of microwaves in the regeneration of sorbents. These include reactor type, sorbent dielectric properties and process design. They found that because of the limited penetration depth of microwave radiation (in the cm range), thin, annular beds or fluidised beds are the favoured reactor types. More recently, microwave desorption was investigated for the regeneration of amine solutions [23,24] and sorbents [25–27] used in post-combustion CO_2 capture.

Microwave desorption of solid sorbents has some favourable characteristics compared to traditional TVSA cycles. Cherbański and Molga [22] discuss various examples of processes where microwave heating is both faster and more efficient than traditional heating. Chronopoulos et al. [25] show that microwave desorption of CO_2 from activated carbon at moderate temperatures (70 °C and 130 °C) is three to four times faster than conventional thermal desorption under similar circumstances. Nigar et al. [26] use an amine-functionalised silica sorbent for CO_2 capture from flue-gas. They suggest that the polar amine-groups selectively absorb microwave radiation, leading to more efficient energy use than conventional desorption. Microwave desorption was also found to be four times faster than TSA.

Meloni et al. [28] found that the reactor geometry is an important factor in the design of a microwave desorber, mainly because the geometry largely determines how much radiation is reflected to the microwave generator (and consequently lost). They found that microwave desorption is faster and more energy efficient than conventional TSA, with an efficiency up to 75%. Ellison et al. [27] show that microwave desorption of CO_2 from zeolite 13X under flue-gas capture conditions is at least twice as fast as conventional desorption. The potential benefits microwave heating are clear: more uniform, faster and more efficient heating compared to traditional TVSA processes.

The aforementioned publications all consider CO_2 capture from flue gases using zeolites [27,28], activated carbon [25] (which are known good microwave absorbers) or a custom functionalised silica sorbent [26]. In the context of direct air capture (DAC), however, desorption is also a key step determining the largest part of the energy consumption [13,29–31]. Microwave desorption could therefore also benefit DAC processes. The sorbents discussed before, however, have poor performance under air capture conditions because of the much lower CO_2 concentration (410 ppm v.s. 10–15 vol.%). For air capture, supported amine sorbents are usually used. The present work therefore investigates if microwave regeneration is feasible for a DAC process using an unmodified, commercial supported amine sorbent (SAS).

2. Theory

As a commercial sorbent Lewatit VP OC 1065 (benzylamine-functionalised, porous polystyrene particles) is considered in this work since it is widely used for DAC, both in previous works of our group [31–33] as well as outside [15,16,30,34]. Consequently, many properties including CO_2 and water isotherms are already known. In this work, the CO_2 isotherm model by Bos et al. [11] was used. To describe the water adsorption equilibrium, the Guggenheim–Anderson-de Boer (GAB) isotherm was fitted to the data from Veneman et al. [35] (Eqs. (1)–(3), see Table 1). In these equations, ϕ is the relative humidity. It is well-known that co-adsorption of water on amine sorbents increases the CO_2 equilibrium capacity [13,35]. However, since in this work no detailed modelling of the adsorber is done and the isotherm is only used to estimate the initial CO_2 loading at the desorption start, this effect is not taken into account. The sorbent is thermally stable in up to 70 °C when oxygen is present, and up to 120 °C in oxygen-lean atmospheres [12]. Above these temperatures, rapid degradation resulting in a CO_2 capacity loss occurs.

$$q_{H_2O} = C_m \frac{C_G K_{ads} \phi}{(1 - K_{ads}\phi)(1 + (C_G - 1)K_{ads}\phi)} \quad (1)$$

$$C_G = C_0 \exp\left(\frac{\Delta_c H}{RT}\right) \quad (2)$$

Table 1
GAB water isotherm parameters.

Parameter	Value
C_m	3.845 mol kg^{-1}
C_0	1.382×10^{-6}
K_0	0.7983
$\Delta_c H$	39.8 kJ mol^{-1}
$\Delta_k H$	– 0.116 kJ mol^{-1}

$$K_{ads} = K_0 \exp\left(\frac{\Delta_k H}{RT}\right) \quad (3)$$

For the optimal absorbance of microwave radiation by the sorbent particles, it is key that the dielectric loss factor is low. Although this may seem counter-intuitive, a lower loss factor is beneficial for the even absorbance of microwave radiation. If the loss factor is high, all radiation will be absorbed in the bed close to where radiation enters the cavity, as if the radiation behaves like a beam of particles. When the dielectric loss factor is low, however, little radiation is absorbed when the radiation first encounters the bed. The microwaves go through the bed with little loss, are reflected against the walls of the cavity, creating an interference pattern. Since the radiation now fills the entire cavity (albeit with standing waves, leading to an inhomogeneous electric field), the complete bed of sorbent is heated, due to the fact that the dielectric loss factor is low [36].

3. Modelling

From the works of Cherbański and Molga [22] and Meloni et al. [28] it is known that the geometry of the desorber is of key importance to its performance for microwave desorption. To aid the design of the desorber an electromagnetic model was made using the electromagnetic waves module in COMSOL Multiphysics version 5.5. A radial-flow configuration was chosen for the desorber, based on previous experience with this reactor configuration [32] and because the bed can be kept thin in this case, which is favourable for microwave penetration [22]. The configuration designed allows for both fixed-bed and moving-bed operation where in the latter case there is a continuous flow of sorbent.

The power dissipation inside the sorbent bed P_d is of interest to assess the desorber performance. P_d is a function of the root mean square electric field strength (E_{rms}) according to Eq. (4) [37]. Since the field strength can vary across the domain, so can the power dissipation and thus heating inside the domain is not necessarily uniform. It is therefore important to model the electric field inside the desorber to assess if significant hot spots will occur. This is especially important for batch operation, since during continuous operation the sorbent itself will move through the bed and will therefore not stay in high power dissipation zones for long times.

$$P_d = 2\pi f \varepsilon_0 \varepsilon'' E_{rms}^2 \quad (4)$$

In order to model the electric field in the sorbent bed, its dielectric properties are required. Since no data on the dielectric constant of Lewatit VP OC 1065 was available in literature and no equipment was available to measure it, an approximation of this property was made. For polystyrene (the sorbent backbone) and benzylamine (the functional group) the dielectric data is available in literature (see Table 2). The Landau-Lifshitz-Looyenga (Eq. (5)) was then used to approximate the dielectric properties of the sorbent [38]. In this equation the subscript 's' denotes the sorbent, 'ps' polystyrene and 'ba' benzylamine and ν denotes a volume fraction. From the work of Yu et al. [12] it is known that the amine loading is 6.8mol/$kg_{sorbent}$. This amounts to a benzylamine mass fraction of 73%. Because of the similar molar mass of benzylamine and styrene (107.15 g mol^{-1} vs. 104.14 g mol^{-1}) it is assumed that the volume fraction of benzylamine also equals 73%. The calculated value for ε_s for a solid polystyrene/mixture was then compensated for the porosity of the sorbent particles itself (0.23) [39] and the sorbent bed (0.39) [40] by again applying Eq. (5). This allows the dielectic properties of Lewatit VP OC 1065 to be approximated.

Table 2
Dielectric properties of polystyrene, benzylamine, water and Lewatit VP OC 1065 (approximated) at 25 °C and 2.45 GHz.

Substance	ε'	ε''	tanδ	Source
Polystyrene	2.55	8.0×10^{-4}	3.0×10^{-4}	[36]
Benzylamine	5.0	0.4	0.08	[41]
Water	76.7	12	0.16	[37]
Lewatit VP OC 1065	4.28	0.27	0.06	(calculated with Eq. (5))

$$\varepsilon_s = \varepsilon_s' - i\varepsilon_s'' = \left(\nu_{ps}\varepsilon_{ps}^{\frac{1}{3}} + \nu_{ba}\varepsilon_{ba}^{\frac{1}{3}}\right)^3 \quad (5)$$

Figs. 1 and 2 schematically show the desorber geometry. The height of the desorber (h_d) is not shown in this picture. The waveguide (WR-340, 86.36 mm × 43.18 mm) enters the reactor at half the height. Microwave radiation enters the waveguide in transverse electric mode 10 with a zero phase-angle. The microwave frequency and input power were fixed to 2.45 GHz and 1.0 kW. The bed thickness t_{bed} was fixed to 10 mm, which is smaller than the microwave penetration depth but still thick enough to allow for an even gas and sorbent flow. The remainder of the dimensions (d_o, d_i, h_d) were varied in the ranges shown in Table 3. l_{wg} was also varied, but had no significant influence on the results. The electric field was then solved using COMSOL Multiphysics (electromagnetic waves module) assuming temperature independent properties. Using the model, the energy absorbance by the sorbent bed was calculated. In these simulations the resistive losses by the steel outer wall (with an electrical conductivity $\sigma = 6.29\,MS\,m^{-1}$) were taken into account. The optimum desorber dimensions were then obtained from the simulation with the highest energy absorbance (993 W out of 1000 W input). Of the 7 W not absorbed by the sorbent, 6 W was absorbed by the steel wall and only 1 W was reflected back to the generator. The optimal dimensions are all multiples of half the microwave wavelength. This is expected, as in a cavity with such dimensions the required standing wave pattern is formed most effectively, leading to the highest field strength and power dissipation [36].

Fig. 2 shows the modelled power dissipation in the sorbent bed with the optimal geometry. It is clear that the power dissipation is not entirely uniform: it varies from almost zero in some places in the domain to about 2 MW m^{-3} in others. In the centre, near the waveguide inlet and at the top and bottom of the desorber there are four hot spots distributed along the radial axis of the bed. In between there are two cold 'bands'. During batch operation (with the sorbent stationary) it is expected that, because of the nonuniform power dissipation the desorber performance is negatively affected. For continuous operation (with moving sorbent) this is expected to be less of a problem, because the sorbent will move across spots with various power dissipation values, thus on average experiencing more uniform heating.

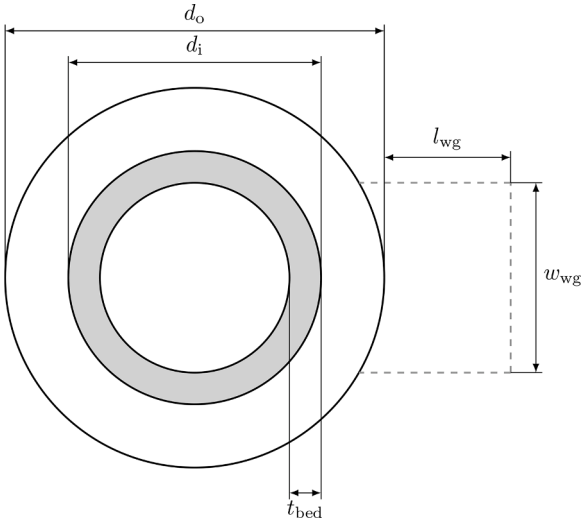

Fig. 1. Schematic top view of the microwave desorber geometry.

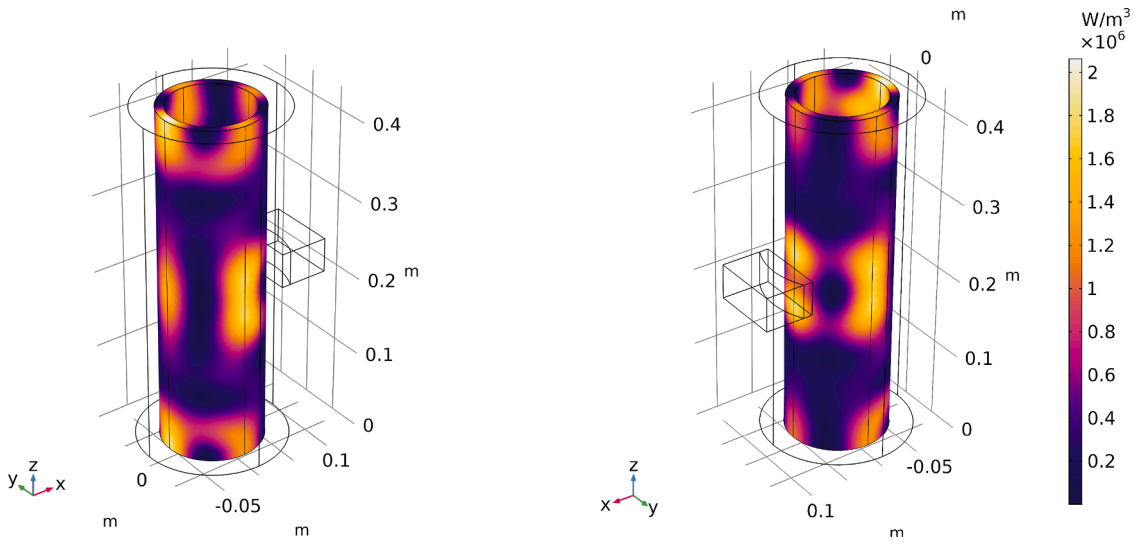

Fig. 2. Modelled power dissipation in the sorbent bed in the optimal geometry, left: front size, right: back side.

Table 3
Ranges of the dimensions varied with the electromagnetic sensitivity study.

Parameter	Lower bound [mm]	Upper bound [mm]	Step size [mm]	Optimum [mm]
d_o	147 (1.2λ)	306 (2.5λ)	12 (0.1λ)	181 (1.5λ)
d_i	51 (0.42λ)	142 (1.16λ)	6.11 (0.05λ)	122 (λ)
h_d	122 (λ)	612 (5λ)	31 (0.25λ)	426 (3.5λ)

Since it was not possible to measure the dielectric properties of the sorbent these were approximated, as mentioned before. To test the effect of this approximation, the dielectric properties of the sorbent were varied from those of pure polystyrene to those of pure benzylamine using Eq. (5). The electric field was then modelled in the optimal configuration (see Table 3) and the total power absorption by the sorbent calculated. Fig. 3 shows the simulated power absorption and calculated loss factor (ε_s'') as function of the benzylamine volume fraction. It is clear that for a benzylamine volume fraction ranging from 0.6 to 1.0, the effect on the power absorption is limited. This shows that the desorber performance is affected little by errors in the approximated dielectric properties. It is, however, desirable to measure these properties for more detailed modelling work in the future.

The effect of adsorbed water on the desorber performance was also assessed, by varying the water loading and calculating the sorbent dielectric properties with the values in Table 2 and applying Eq. (5). The calculated loss factor and simulated power dissipation are shown in Fig. 4. With increasing water loading, the power dissipation first decreases with about 30%, and then increases again towards the maximum value of 1000 W. Adsorbed water does therefore have some effect on the desorption performance, but the effect is limited, especially during moving bed operation.

4. Materials and methods

An experimental setup was constructed based on the basic dimensions found from the electromagnetic simulations (see Fig. 5, P&ID in Fig. 6). The reactor vessel and waveguide were constructed from stainless steel. The top and bottom flanges are sealed using Uvox WMC-2-2-(EM-5-2-4003)-AC seals, which provide both gas- and radiation tightness. The annular space of the bed itself was made from PTFE-coated fiberglass cloth, stretched between two brass rings bolted in the reactor vessel. PTFE-coated glass rings were placed on the inside of the cloth as support. Holes were drilled in the brass rings to allow the sorbent to flow in and out of the bed. On the bottom, two perforated rings were placed on top of each other. By moving the bottom ring relative to the top ring, the sorbent flow could be controlled. This is done via a pneumatic actuator connected to a timer. As purge gas nitrogen is used, the flow of which is controlled via a rotameter (FIC-01). Nitrogen

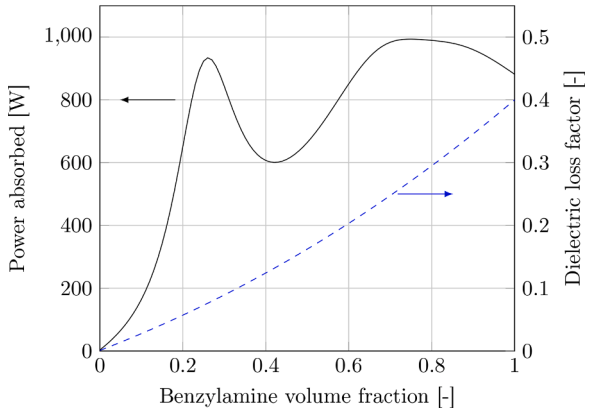

Fig. 3. Simulated power absorption (solid line) and loss factor (dashed line) as function of the benzylamine volume fraction when using Eq. (5) to calculate the sorbent dielectric properties.

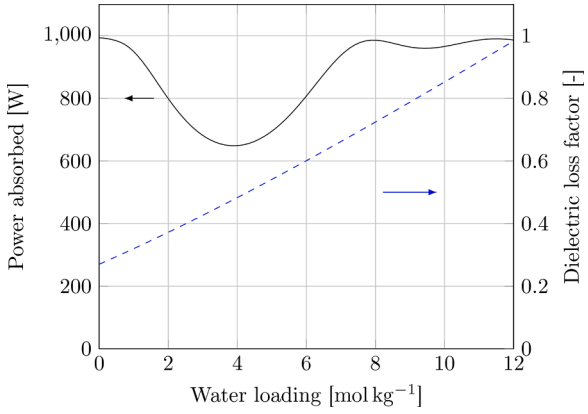

Fig. 4. Simulated power absorption (solid line) and loss factor (dashed line) as function of the water loading when using Eq. (5) to calculate the sorbent dielectric properties.

Fig. 5. Picture of the microwave desorber setup.

is used here to minimise the risk on oxidative degradation of the sorbent. For industrial applications either air as purge gas (while limiting the desorption temperature to 70 °C) to produce enriched air for horticulture applications or vacuum operation without purge gas to produce CO_2 is recommended. The magnetron tube (Hitachi 2M107A) is controlled by a timer to vary the effective power. The outlet gas is analysed with a Sick Maihak Sidor CO_2 analyser (type 760639, XI-01, prior to this excess water is removed in a condenser to prevent condensation in the analyser). The flow through the analyser is controlled to 1 L/min via a rotameter (FIC-02). The temperature of the bed is measured with an IR pyrometer (Calex PC151MT-3) placed in an electromagnetic attenuation duct (TI-01, approximate location see Fig. 7). Furthermore, K-type thermocouples are used to measure the gas outlet temperature (TI-02) and the magnetron temperature (TI-03). The sorbent collection vessel is placed on a balance (Kern DS 20K0.1) to measure the processed sorbent mass over time.

To calculate the energy duty of the system the current going through the magnetron generator was measured using a current clamp (LEM AT 20 420L) which was calibrated using a Fluke 117 True-RMS multimeter. Since the magnetron generator is an inductive load, its power factor ($\cos\varphi$) is required to accurately calculate the energy consumption. This value was measured with a Rigol DS1054 Z oscilloscope and determined to be 0.96. The electrical grid voltage was measured using an Alecto EM-16 power meter. Data from the CO_2 analyser, current clamp and pyrometer was logged every second on a computer via a Picolog 1012 ADC. The thermocouple data was logged every second via a Picolog TC-08 logger also on the computer. The sorbent collector balance reading was manually logged every five minutes during the continuous experiments. The CO_2 analyser was calibrated using pure nitrogen and a 1 vol. % CO_2 in nitrogen calibration gas mixture.

For all experiments the sorbent was adsorbed overnight or longer with ambient air from the High Pressure Laboratory of the University of

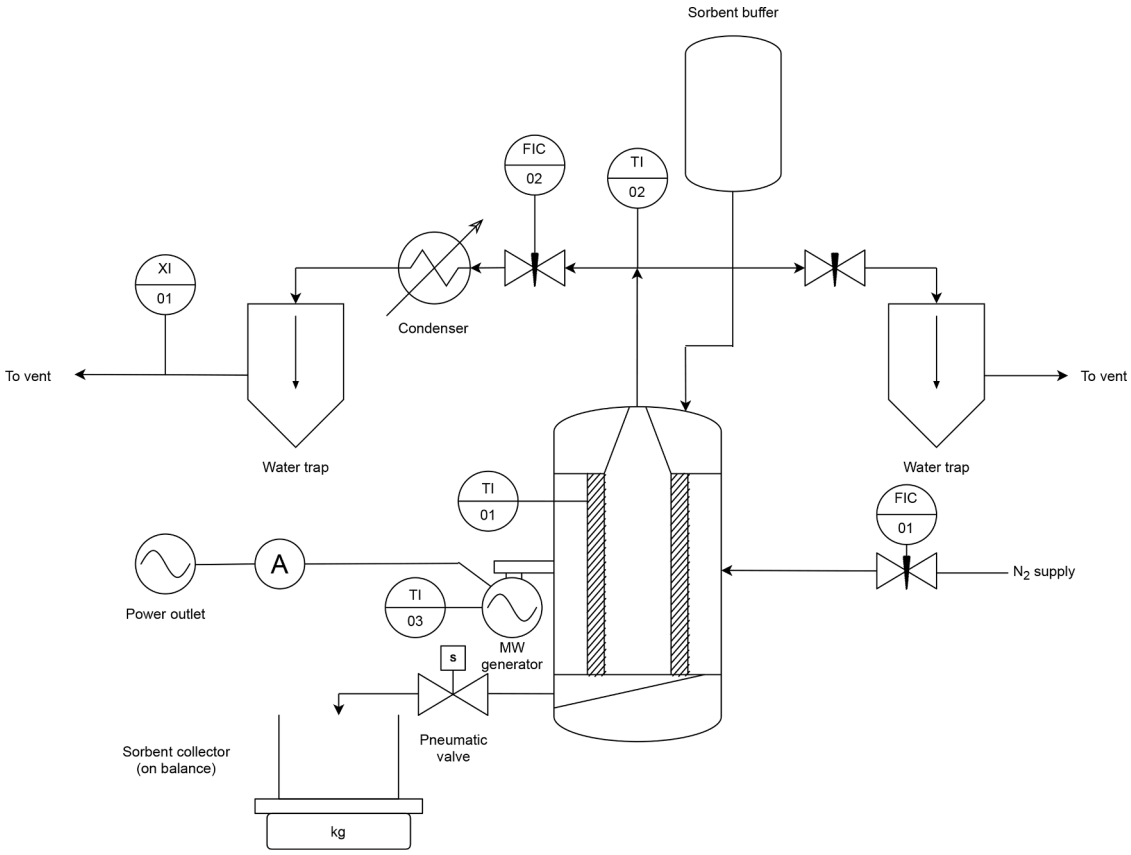

Fig. 6. P&ID of the microwave desorption setup. The hatched area is the sorbent bed.

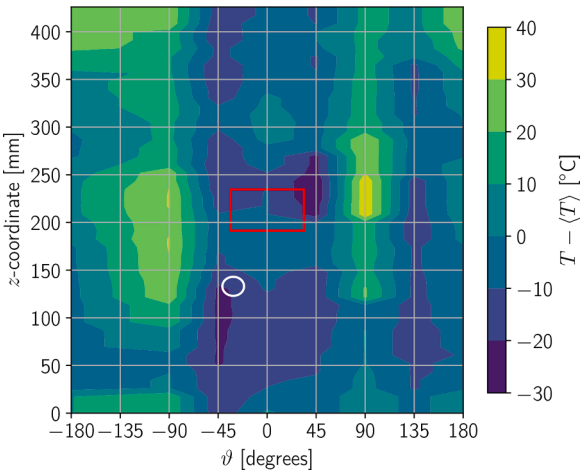

Fig. 7. Measured temperature profile in the bed after a batch desorption run. The red rectangle shows the approximate waveguide position, the white circle shows the approximate IR temperature sensor location. (For interpretation of the references to colour in this figure legend, the reader is referred to the web version of this article.)

Twente (NL). The lab conditions were measured using a RS PRO RS 967 temperature, humidity and CO_2 concentration indicator during adsorption are summarised in Table 4, the CO_2 and water loading values were calculated with the isotherm from Bos et al. [11] and Eq. (1). During batch runs 1 to 3 no environmental data was measured, so these values are estimated based on the weather conditions (as outside air is used for ventilation of the lab). The CO_2 concentration during adsorption before these runs was assumed to be the mean of during adsorption of the continuous runs. The duty cycle of the microwave generator was controlled by setting the on- and off times on a timed switch. The on-time was always 1 min, while the off-time was varied between 2 min to 3 min. For the batch experiments the reactor was filled with sorbent which remained inside the reactor for the entire experiment duration. Prior to the continuous experiments, the sorbent buffer vessel was filled with adsorbed sorbent. The sorbent flow was then controlled by a timer-controlled pneumatic actuator. Here, the open-time was always 1 s while the closed-time varied between 18 s to 36 s. The batch experiments were done until the bed temperature exceeded 100 °C or the outlet CO_2 concentration dropped below 1 vol.%. The continuous experiments were done until the sorbent buffer vessel (containing 3 kg to 4 kg sorbent at the start) was empty. The experimental parameters of the batch and continuous experiments are shown in Tables 5 and 6.

Data processing was done with Python 3.6 and NumPy 1.19.5. The amount of CO_2 desorbed over time (n_{CO_2}) was calculated from the analyser output and nitrogen inlet gas flow ($\phi_{V,in}$) via Eq. (6) where p_{amb} and T_{amb} denote the ambient pressure and temperature. The mean productivity was calculated by time-averaging the CO_2 outlet flow over the time interval from the experiment start to until the microwave generator was turned off. The sorbent loading over time (or loading difference over time for the continuous experiments) was calculated by dividing this value by the amount of sorbent (batch) or the cumulative sorbent mass processed (continuous). The total power input (Q_{elec}) was calculated from the current clamp reading with Eq. (7). On the same power outlet the cooling fan for the magnetron was connected, using a constant current of 0.43 A. The microwave current was then determined as the input current from the current clamp minus the fan current. The fan duty (Q_{fan}) itself is calculated as $U_{net}I_{fan}t$. The nitrogen purge gas enters the reactor cold, but is heated inside. The sensible heat associated with this ($Q_{sens,gas}$) is calculated with Eq. (8) assuming a constant specific heat capacity. The sensible heat taken up by the bed itself ($Q_{sens,bed}$) is calculated with Eq. (9), where m_{bed} is the amount of sorbent initially in the bed (0.782 kg) and $m_{s,t}$ the cumulative sorbent mass processed (0 for batch experiments). The CO_2 and water desorption energy consumption ($Q_{CO_2,des.}$ and $Q_{H_2O,des}$) were calculated with Eqs. (10) and (11), where n_{CO_2} was calculated with Eq. (6) and n_{H_2O} was calculated from the Eq. (1) and the processed sorbent mass assuming full water desorption during the experiment. Finally, the energy losses (Q_{loss}) were calculated with Eq. (12). All energy duties calculated are normalised by the amount of CO_2 produced to yield a value in MJ/kg CO_2.

Table 5
Conditions and results of batch desorption experiments.

Run #	Gas flow [L/min]	Duty cycle [%]	Energy duty [MJ/kg CO_2]	Mean productivity [kg CO_2/d]
1	12	25	25.4	1.05
2	28	25	24.2	1.20
3	28	33	26.4	1.52

$$n_{CO_2} = \frac{\phi_{V,in}p_{amb}}{RT_{amb}}\int_0^t \frac{x_{CO_2,out}}{1-x_{CO_2,out}}\mathrm{d}t \tag{6}$$

$$Q_{elec} = \int_0^t U_{net}I_{total}\cos\varphi \mathrm{d}t \tag{7}$$

$$Q_{sens,gas} = \frac{\phi_{V,in}p_{amb}M_{w,N_2}C_{p,N_2}}{RT_{amb}}\int_0^t \left(T_{gas,out}-T_{gas,in}\right)\mathrm{d}t \tag{8}$$

$$Q_{sens,bed} = \left(m_{bed}+m_{s,t}\right)C_{p,bed}\left(T_{bed,t}-T_{bed,0}\right) \tag{9}$$

$$Q_{CO_2,des} = n_{CO_2}\Delta_{ads}H_{CO_2} \tag{10}$$

$$Q_{H_2O,des} = n_{H_2O}\Delta_{ads}H_{H_2O} \tag{11}$$

$$Q_{loss} = Q_{elec} - Q_{fan} - Q_{CO_2,des} - Q_{H_2O,des} - Q_{sens,gas} - Q_{sens,bed} \tag{12}$$

Table 4
Environmental conditions in the High Pressure Laboratory of the University of Twente (NL) at the end of sorbent adsorption. Values marked with an asterisk were estimated using nearby weather station data. The CO_2 and water loading were calculated using the Tóth isotherm [11] and Eq. (1).

Experiment	Date	Temperature [°C]	Humidity [% RH]	CO_2 conc. [ppm]	q_{CO_2} [mol kg^{-1}]	q_{H_2O} [mol kg^{-1}]
Batch #1	10-12-2020	12*	30*	486*	1.55	4.44
Batch #2	14-12-2020	15*	50*	486*	1.45	5.80
Batch #3	15-12-2020	15*	50*	486*	1.45	5.80
Continuous #1	25-03-2021	20.4	40	556	1.33	4.85
Continuous #2	26-03-2021	19.2	45	507	1.33	5.26
Continuous #3	31-03-2021	18.9	39	515	1.35	4.81
Continuous #4	22-04-2021	13.2	37	415	1.46	4.88
Continuous #5	04-05-2021	16.6	46	437	1.37	5.46
Continuous #6	11-05-2021	17.3	43	473	1.37	5.19

Table 6
Conditions and results of continuous desorption experiments. During run 3 the duty cycle started at 33%, but was lowered to 25% because the bed temperature became too high.

Run #	Sorbent processed [kg]	Sorbent flow [g/min]	Gas flow [L/min]	Sorbent residence time [min]	Duty cycle [%]	Energy duty [MJ/kg CO_2]	Mean productivity [kg CO_2/d]
1	2.0	32.9	22	23.8	25	38.3	0.70
2	1.3	13.8	22	56.6	25	30.8	0.86
3	1.9	14.8	22	52.9	25	29.9	1.00
4	2.7	15.8	20	49.4	25	47.3	0.55
5	2.7	18.7	30	41.9	25	25.5	1.01
6	2.8	52.3	30	15.0	33	32.3	1.27

4.1. Sorbent characterization

During the experimental campaign the sorbent was characterised twice using a Netzsch STA 449 F3 Jupiter thermogravimetric analyzer. In the device, the sorbent was first desorbed under nitrogen flow and 120 °C for six hours. Then, the sorbent was cooled down to 40 °C and exposed to 15 vol.% CO_2 in nitrogen for four hours. The sample mass was continuously measured and from this the sorbent equilibrium CO_2 loading was calculated. The first sample was analysed before the batch experiments (which were done before the continuous runs). This sample had an equilibrium loading which matched the isotherm very well. The second sample was analysed after continuous run #3. This sample showed signs of degradation: the CO_2 loading was about 15% lower than predicted by the isotherm. This indicates that some thermal degradation of the sorbent has occurred during the batch or first continuous experiments, possibly due to local hot spots in the bed.

5. Results and discussion

5.1. Bed temperature profile

The temperature distribution in the sorbent bed was determined by, at the end of a batch desorption experiment, quickly opening the reactor and scanning the bed with the pyrometer at different angles (relative to the waveguide). The mean temperature was subtracted from the measured values, which were then linearly interpolated and plotted in Fig. 7 as function of the angle relative to the waveguide and the bed height. In this figure, the waveguide location is indicated by the red square. It is clear the temperature distribution is nonuniform: the lowest and highest temperature value are 70 °C apart. There are two warmer 'bands' at − 90° and +90°, which correspond to those in the simulated power dissipation in Fig. 2. The hot spots at the bottom and top of the domain also exist in the simulated power dissipation distribution. During the continuous experiments the heat distribution is expected to be more uniform, since then the sorbent moves through the domain.

5.2. Batch experiment results

Experiments in batch mode were done at the two gas flows and two duty cycles, as shown in Table 5. This table also summarises the mean CO_2 productivity and the minimum energy duty found during the experiment. Fig. 8 shows the CO_2 desorption progress during the experiments over time and Fig. 9 the energy duty normalised by the amount of CO_2 desorbed. From Fig. 8 it is clear that, after the initial heating up of the sorbent, desorption continues steadily until (almost) all adsorbed CO_2 is released. The amount of CO_2 desorbed varies per run, most probably due to different adsorption conditions and times. Run 3 yields the fastest desorption rate, which is expected because during this run the magnetron duty cycle and nitrogen gas flow are highest. In Fig. 10 the sorbent bed temperature is plotted over time. Clearly during runs 1 and 2 (both with a 25% duty cycle) the temperature profile is very similar, while during run 3 the temperature rises more quickly due to the higher duty cycle (33%). Fig. 9 shows that over time the desorption cumulative energy duty decreases until a minimum value, after which it slowly increases again. This is because initially the sorbent has to heat up and water is desorbed (which requires energy, while little CO_2 is produced). At the end of the experiment, the CO_2 production drops (because desorption is almost complete), while the magnetron energy input remains similar, explaining the increase in energy duty after the minimum. The minimum energy duty required for desorption is similar for all batch experiments and amounts to around 25 MJ /kg CO_2.

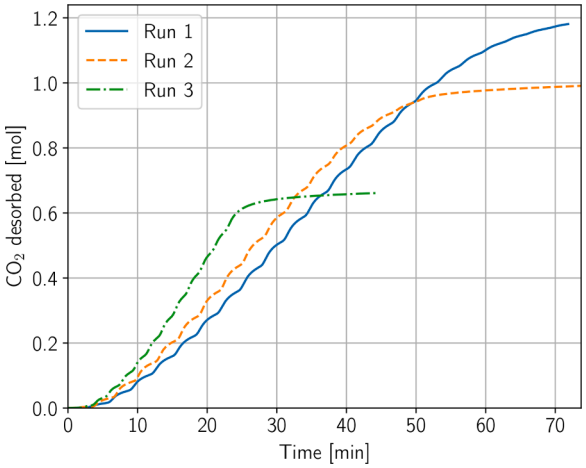

Fig. 8. CO_2 desorption progress during batch desorption.

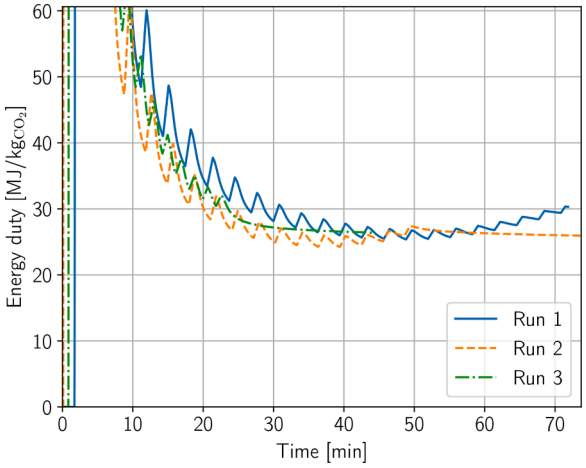

Fig. 9. Cumulative total energy duty, normalised by cumulative CO_2 production during batch desorption.

5.3. Continuous experiment results

Beside the batch fixed-bed experiments, continuous experiments with a moving sorbent bed were done. These experiments were done

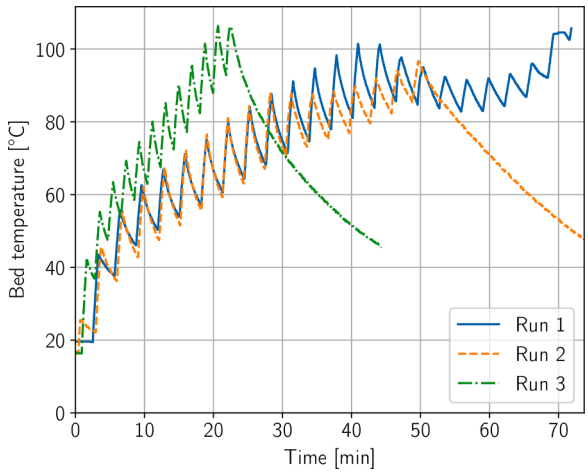

Fig. 10. Bed temperature during batch desorption.

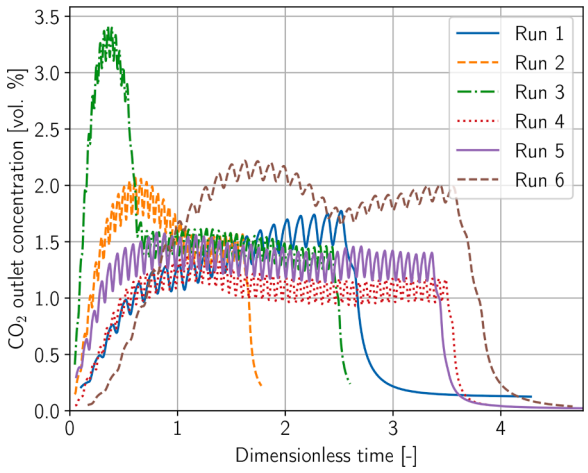

Fig. 12. CO_2 outlet concentration during continuous desorption.

until all sorbent in the buffer vessel was processed. Hence, the experiment time depends highly on the sorbent flow rate. To better compare the results, the results are plotted against the dimensionless time defined as t/τ_{sorbent}. Table 6 shows the experimental parameters during the six continuous experiments and summarises some key performance parameters. The cumulative CO_2 production is plotted in Fig. 11. During run 3 the duty cycle at the start was 33%, but it was lowered to 25% since the bed temperature became too high (see Fig. 13). In the curve of run 3 this effect is visible at a dimensionless time of about 0.5. In all experiments a short time was required to heat up the bed to the point where CO_2 desorption commenced. At the end of each experiment the sorbent flow was stopped and the microwave was turned off, while the gas flow remained on. This was done to remove and measure the CO_2 still in the reactor vessel at the end of the experiment. The total amount of CO_2 produced varies between the experiments, since the conditions during adsorption and amount of sorbent processed were not equal (see Tables 4 and 6).

Fig. 12 shows the CO_2 outlet concentration over time. A moving average filter with a window size of 30 s was applied to the data to filter out the large fluctuations due to the magnetron duty cycle. With the exception of run 3, the trends look similar. The CO_2 outlet concentration is roughly between 1 and 2 vol.%, which is suitable for e.g. enhancing algae growth or horticulture applications. During all runs, the CO_2 outlet concentration converges to a more-or-less constant value after a dimensionless time of 1 to 1.5.

Fig. 13 displays the bed temperature over time, processed with a moving average filter with a window size of 30 s. It is clear that during run 3 the temperature became too high, so that the magnetron duty cycle had to be reduced to prevent damage to the sorbent. The 'steady state' temperature during run 2, 3, 4 and 5 has a similar value around 95 °C. During these experiments the sorbent flow was approximately equal (see Table 6). The same holds for runs 1 and 6: with a similar sorbent flow, a similar steady-state temperature is reached. This observation indicates that it is important to match the sorbent flow to the energy input from the magnetron or vice versa to prevent overheating, but still allow as fast as possible desorption.

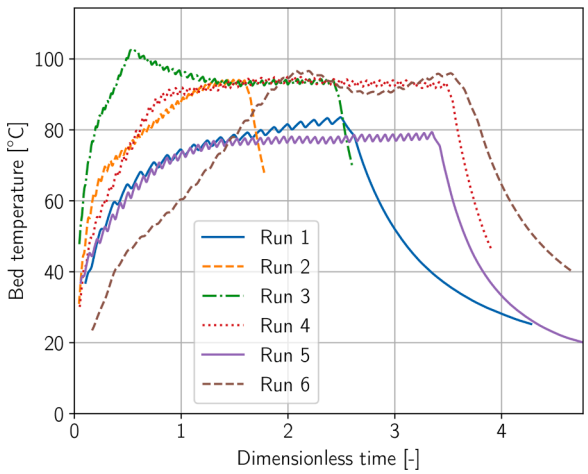

Fig. 13. Bed temperature during continuous desorption.

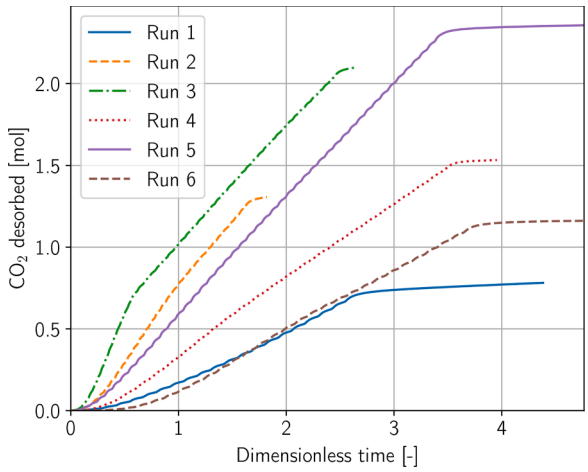

Fig. 11. CO_2 desorption progress during continuous desorption.

In Fig. 14 the cumulative desorption energy duty is plotted over time. All runs have a similar trend: the energy duty starts high (since it takes some time before CO_2 desorption commences, because the bed has to heat up first) and decays to a 'steady-state' value. The minimum energy duty for runs 2, 3, 5 and 6 is very similar and around 25 MJ/kg CO_2 to 30 MJ/kg CO_2. Run 4 has a much higher energy duty. During this experiment the mean CO_2 productivity and the mean CO_2 outlet concentration is also much lower (see Table 6). This could be caused by an incomplete adsorption saturation of the sorbent, an excessively inhomogeneous electric field or an inhomogeneous flow of the sorbent.

5.4. Energy duty breakdown

To assess the efficiency of the process, the total energy duty is broken down into the different contributions via Eqs. (7)–12. For the batch experiments, this is shown in Fig. 15. The water desorption energy varies

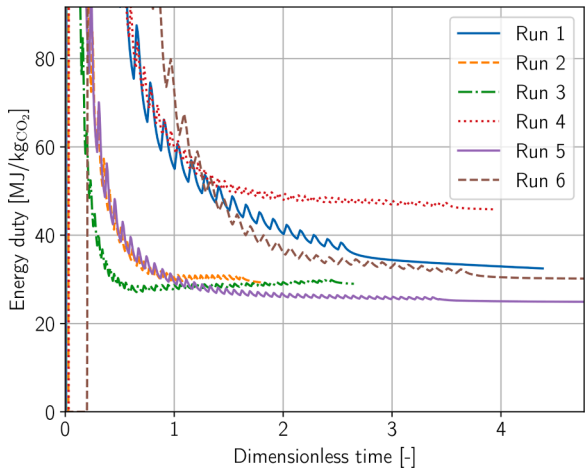

Fig. 14. Cumulative energy duty, normalised by cumulative CO_2 production during continuous desorption.

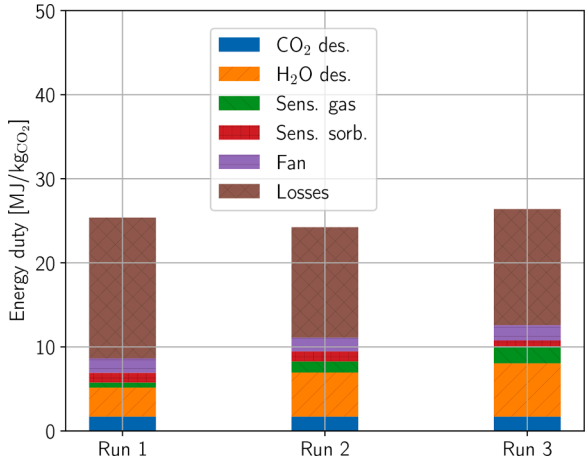

Fig. 15. Breakdown of energy duty during batch desorption experiments.

significantly between the experiments, due to the different relative humidity during the adsorption of the sorbent and consequently, the different initial water loading. Furthermore, the gas sensible heat contribution varies considerably because of the different gas flows and the different gas outlet temperature.

Fig. 16 breaks down the energy duty for the continuous experiments.

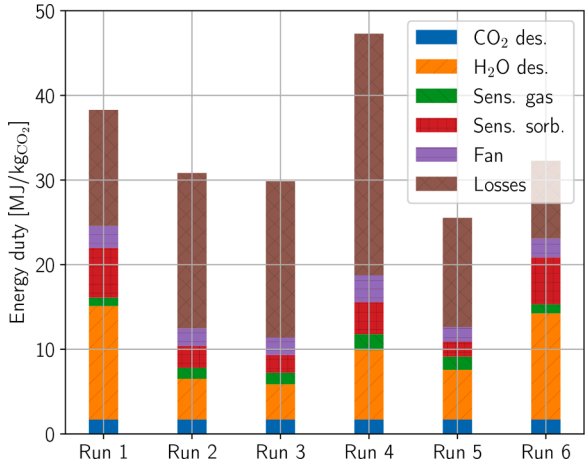

Fig. 16. Breakdown of energy duty during continuous desorption experiments.

A few things stand out in the comparison between the different experimental runs. First of all, the water desorption energy varies greatly between the different experiments showing the importance of the humidity during adsorption on the energy duty of the process. Second, the sorbent sensible heat during run 1 and 6 is significantly greater than the other runs. This is due to the higher sorbent flow (and lower working capacity) as can be seen in Table 6. Third, the losses are very different across the different runs. Part of this may be attributed to the power reflected back to the microwave, which can depend on the distribution of the sorbent in the bed, the sorbent loading and possibly the temperature. Other causes could be a different electric field distribution or a different sorbent residence time distribution.

5.5. Comparison to traditional desorption

The results of the present work are compared to literature results on traditional desorption processes for DAC. Wurzbacher et al. [13] did experiments and simulations of TVSA desorption of an amine-functionalised cellulose sorbent. Their small fixed-bed batch experiments showed that (depending on the amount of water adsorbed on the sorbent) 60 min to 120 min is required before 90% of the final temperature is achieved. In the present work, the time to achieve this in the batch experiments ranges from 20 min to 40 min (see Fig. 10), indicating much faster heating and consequently faster desorption. Bajamundi et al. [29] did experiments with a pilot-scale DAC setup under real-life conditions, using a TVSA cycle. They found an energy duty of 36MJ/kg CO_2, taking into account all losses and including the adsorption phase. This is slightly higher than the duty found in the present work (see Table 5 and Table 6), although in the present work no adsorption is taken into account. The desorption productivity (e.g. CO_2 productivity if the adsorption time is not taken into account) was 0.067kg $CO_2/kg_{sorb.}/d$. In the present work (taking batch run #2 as an example) this amounts to 1.5 kg $CO_2/kg_{sorb.}/d$, which is considerably higher. It must be noted, however, that in the works of Wurzbacher et al. and Bajamundi et al. pure CO_2 is produced via vacuum desorption, while in this work enriched air under ambient pressure is made. It is expected that if vacuum desorption is used and pure CO_2 is made the productivity will increase (because of the lower CO_2 partial pressure) and the energy duty will also increase by 0.5 MJ/kg CO_2 to 2 MJ/kg CO_2 (due to the compression) [31].

Elfving et al. [30] analysed several desorption strategies for desorption of CO_2 from Lewatit VP OC 1065, including TSA and TVSA cycles at different temperatures and with and without a purge gas. Batch desorption experiments were done and the desorption time and energy duty are reported. For a TSA desorption step at 100 °C (which is similar to the experiments in this work) a productivity of 0.39 kg $CO_2/kg_{sorb.}/d$ is calculated by dividing the reported working capacity by the desorption time. This value is about four times lower than the value found in the batch experiments of this work (around 1.5 kg $CO_2/kg_{sorb.}/d$). The energy duty reported is 6.4 MJ/kg CO_2, which is considerably lower than the value in this work. This is most probably because Elfving et al. do not take into account energy losses related to water desorption and energy losses to the environment.

The present results are also compared to previous work within the research group of the authors. Yu and Brilman [32] discuss the design of an air capture setup with a moving bed radial adsorber (not unlike the reactor in the present work) and a fluidised-bed desorber. They report a theoretical energy demand (without losses) of around 6 MJ/kg CO_2, which is considerably lower than in the present work. This can be explained in part by the losses incurred in the present work, and the relatively high humidity encountered during the present experiments. Bos et al. [33] experimentally studied a TVSA cycle using steam as a purge gas to produce pure CO_2 and found energy duties in the range of 10 MJ/kg CO_2 to 55 MJ/kg CO_2, which is comparable to the duties found in this work. Schellevis et al. [31] developed a fixed-bed TVSA

DAC setup and modelled the energy consumption. They found an energy demand for batch desorption (without losses) of around 17 MJ /kg CO_2 for enriched air production at atmospheric pressure using nitrogen as purge gas (which is similar to this work). This value of the energy duty is already reasonably close to the realised values found in this work (which do include losses), which shows the promise of microwave desorption as an efficient alternative for conventional thermal desorption.

5.6. Possible improvements

A significant limitation of the present setup is the inhomogeneity of the electric field in the setup (Fig. 2), which causes hot spots during the desorption process (Fig. 7). Because of this, the magnetron duty cycle has to be limited to prevent local overheating and thermal degradation of the sorbent. This also limits the productivity of the setup. If the field distribution would be improved with, for example, a wavemode stirrer (which homogenizes the electric field) or alternating microwave feed points, significantly higher productivities and possibly better energy efficiencies can be achieved [36]. This is because with a homogeneous electric field and consequently temperature distribution, the desorption rate is no longer limited by the maximum temperature at the hot spots. A future improvement to the process is to modify it for operating under vacuum pressure. If this would be possible, pure CO_2 can be made and the desorption rate can possibly be improved even further. In the current setup the microwave duty cycle is fixed by the timer settings. To improve the desorption performance, the microwave duty cycle should be controlled by the bed temperature. This allows the setup to operate at sufficiently high temperatures to accelerate desorption, but prevent overheating. Finally, some sorbent degradation was observed during the experiments. It is expected that this is caused by local temperature hot spots in the bed, but further research is required to confirm this is not an effect of the microwave radiation itself.

6. Conclusion

The present paper presents a proof-of-concept of a radial-flow microwave desorber using an unmodified commercial amine-functionalized sorbent. The results show that quick sorbent heating and consequently fast desorption is possible. Microwave heating thus bypasses the poor thermal conductivity of the sorbent, which would otherwise limit the desorption rate during conventional desorption. Productivities of up to 1.6 kg $CO_2/kg_{sorb.}/d$ (with 1% to 2% CO_2 in nitrogen) are achieved, both during batch and continuous desorption experiments. This is significantly faster than traditional desorption. The regeneration energy duty is around 25 MJ/kg CO_2 for batch desorption and 25 MJ/kg CO_2 to 50 MJ/kg CO_2 for continuous desorption, with energy losses between 35% and 70%. During the electromagnetic simulations and experiments it was found that the electric field and temperature distributions were not completely uniform, negatively affecting the desorption rate and energy efficiency. Overall, microwave desorption shows promise for enhancing the productivity and energy efficiency of sorbent-based direct air capture.

Declaration of Competing Interest

The authors declare that they have no known competing financial interests or personal relationships that could have appeared to influence the work reported in this paper.

Acknowledgements

The authors thank Benno Knaken, Johan Agterhorst and Ronald Borst (Sustainable Process Technology group, University of Twente) for their invaluable skills and efforts in constructing the experimental setup. This research did not receive any specific grant from funding agencies in the public, commercial, or not-for-profit sectors.

References

[1] K.S. Lackner, H.-J. Ziock, P. Grimes, Carbon capture from air, is it an option?. Conference: 24th Annual Technical Conference on Coal Utilization and Fuel Systems, Clearwater, FL, 1999.
[2] J.G.J. Olivier, J.A.H.W. Peters, Trends in Global CO_2 and Total Greenhouse Gas Emissions: 2020 Report. Technical Report, PBL Netherlands Environmental Assessment Agency, The Hague, 2020.https://www.pbl.nl/sites/default/files/downloads/pbl-2020-trends-in-global-co2-and-total-greenhouse-gas-emissions-2019-report_4068.pdf
[3] J. Rogelj, D. Shindell, K. Jiang, S. Fifita, P. Forster, V. Ginzburg, C. Handa, H. Kheshgi, S. Kobayashi, E. Kriegler, L. Mundaca, R. Séférian, M.V. Vilariño, Mitigation pathways compatible with 1.5 °C in the context of sustainable development, in: V. Masson-Delmotte, P. Zhai, H.O. Pörtner, D. Roberts, J. Skea, P. R. Shukla, A. Pirani, W. Moufouma-Okia, C. Péan, R. Pidcock, S. Connors, J.B. R. Matthews, Y. Chen, X. Zhou, M.I. Gomis, E. Lonnoy, T. Maycock, M. Tignor, T. Waterfield (Eds.), Global Warming of 1.5 °C. An IPCC Special Report on the Impacts of Global Warming of 1.5 °C Above Pre-Industrial Levels and Related Global Greenhouse Gas Emission Pathways, in the Context of Strengthening the Global Response to the Threat of Climate Change, Intergovernmental Panel on Climate Change, 2018.
[4] J.K. Stolaroff, D.W. Keith, G.V. Lowry, Carbon dioxide capture from atmospheric air using sodium hydroxide spray, Environ. Sci. Technol. 42 (8) (2008) 2728–2735, https://doi.org/10.1021/es702607w.
[5] F. Barzagli, C. Giorgi, F. Mani, M. Peruzzini, et al., Screening study of different amine-based solutions as sorbents for direct CO_2 capture from air, ACS Sustain. Chem. Eng. 8 (37) (2020) 14013–14021, https://doi.org/10.1021/acssuschemeng.0c03800.
[6] M. Yang, C. Ma, M. Xu, S. Wang, L. Xu, et al., Recent advances in CO_2 adsorption from air: a review, Curr. Pollut. Rep. 5 (4) (2019) 272–293, https://doi.org/10.1007/s40726-019-00128-1.
[7] X. Shi, H. Xiao, H. Azarabadi, J. Song, X. Wu, X. Chen, K.S. Lackner, et al., Sorbents for the direct capture of CO_2 from ambient air, Angew. Chem. - Int. Ed. 59 (18) (2020) 6984–7006, https://doi.org/10.1002/anie.201906756.
[8] E.S. Sanz-Pérez, C.R. Murdock, S.A. Didas, C.W. Jones, et al., Direct capture of CO_2 from ambient air, Chem. Rev. 116 (19) (2016) 11840–11876, https://doi.org/10.1021/acs.chemrev.6b00173.
[9] J.C. Minx, W.F. Lamb, M.W. Callaghan, S. Fuss, J. Hilaire, F. Creutzig, T. Amann, T. Beringer, W. de Oliveira Garcia, J. Hartmann, T. Khanna, D. Lenzi, G. Luderer, G. F. Nemet, J. Rogelj, P. Smith, J.L. Vicente Vicente, J. Wilcox, M. del Mar Zamora Dominguez, et al., Negative emissions—Part 1: research landscape and synthesis, Environ. Res. Lett. 13 (6) (2018) 063001, https://doi.org/10.1088/1748-9326/aabf9b.
[10] X. Wang, C. Song, Carbon capture from flue gas and the atmosphere: aperspective, Front. Energy Res. 8 (December) (2020), https://doi.org/10.3389/fenrg.2020.560849.
[11] M.J. Bos, T. Kreuger, S.R.A. Kersten, D.W.F. Brilman, et al., Study on transport phenomena and intrinsic kinetics for CO_2 adsorption in solid amine sorbent, Chem. Eng. J. (November) (2018) 0–1, https://doi.org/10.1016/j.cej.2018.11.072.
[12] Q. Yu, J.da la P. Delgado, R. Veneman, D.W.F. Brilman, et al., Stability of a benzyl amine based CO_2 capture adsorbent in view of regeneration strategies, Ind. Eng. Chem. Res. 56 (12) (2017) 3259–3269, https://doi.org/10.1021/acs.iecr.6b04645.
[13] J.A. Wurzbacher, C. Gebald, S. Brunner, A. Steinfeld, et al., Heat and mass transfer of temperaturevacuum swing desorption for CO_2 capture from air, Chem. Eng. J. 283 (2016) 1329–1338, https://doi.org/10.1016/j.cej.2015.08.035.
[14] M.J. Bos, V. Kroeze, S. Sutanto, D.W.F. Brilman, et al., Evaluating regeneration options of solid amine sorbent for CO_2 removal, Ind. Eng. Chem. Res. 57 (32) (2018) 11141–11153, https://doi.org/10.1021/acs.iecr.8b00768.ISSN 0888-5885
[15] E. Sonnleitner, G. Schöny, H. Hofbauer, Assessment of zeolite 13X and Lewatit® VP OC 1065 for application in a continuous temperature swing adsorption process for biogas upgrading, Biomass Convers. Biorefinery 8 (2) (2018) 379–395, https://doi.org/10.1007/s13399-017-0293-3.
[16] J.F. Horstmeier, A. Gomez Lopez, D.W. Agar, Performance improvement of vacuum swing adsorption processes for CO_2 removal with integrated phase change material, Int. J. Greenh. Gas Control 47 (2016) 364–375, https://doi.org/10.1016/j.ijggc.2016.02.013.
[17] X. Shi, H. Xiao, K. Kanamori, A. Yonezu, K.S. Lackner, X. Chen, et al., Moisture-driven CO_2 sorbents, Joule 4 (8) (2020) 1823–1837, https://doi.org/10.1016/j.joule.2020.07.005.
[18] X. Zhu, T. Ge, F. Yang, R. Wang, et al., Design of steam-assisted temperature vacuum-swing adsorption processes for efficient CO_2 capture from ambient air, Renew. Sustain. Energy Rev. 137 (July 2020) (2021) 110651, https://doi.org/10.1016/j.rser.2020.110651.
[19] X. Lin, B. Shao, J. Zhu, F. Pan, J. Hu, M. Wang, H. Liu, et al., In situ electromagnetic induction heating for CO_2temperature swing adsorption on magnetic $Fe3O_4$/N-Doped porous carbon, Energy Fuels 34 (11) (2020) 14439–14446, https://doi.org/10.1021/acs.energyfuels.0c02699.
[20] C.A. Grande, A.E. Rodrigues, Electric swing adsorption for CO_2 removal from flue gases, Int. J. Greenh. Gas Control 2 (2) (2008) 194–202, https://doi.org/10.1016/S1750-5836(07)00116-8.
[21] G. Roussy, P. Chenot, Selective energy supply to adsorbed water and non classical thermal process during microwave dehydration of zeolite, J. Phys. Chem. 85 (15) (1981) 2199–2203.
[22] R. Cherbański, E. Molga, Intensification of desorption processes by use of microwaves—An overview of possible applications and industrial perspectives,

Chem. Eng. Process. 48 (1) (2009) 48–58, https://doi.org/10.1016/j.cep.2008.01.004.
[23] S.J. McGurk, C.F. Martín, S. Brandani, M.B. Sweatman, X. Fan, Microwave swing regeneration of aqueous monoethanolamine for post-combustion CO_2 capture, Appl. Energy 192 (2017) 126–133, https://doi.org/10.1016/j.apenergy.2017.02.012.
[24] F. Bougie, X. Fan, Microwave regeneration of monoethanolamine aqueous solutions used for CO_2 capture, Int. J. Greenh. Gas Control 79 (October) (2018) 165–172, https://doi.org/10.1016/j.ijggc.2018.10.008.
[25] T. Chronopoulos, Y. Fernandez-Diez, M.M. Maroto-Valer, R. Ocone, D.A. Reay, CO_2 desorption via microwave heating for post-combustion carbon capture, Microporous Mesoporous Mater. 197 (2014) 288–290, https://doi.org/10.1016/j.micromeso.2014.06.032.
[26] H. Nigar, B. Garcia-Baños, F.L. Peñaranda Foix, J.M. Catalá-Civera, R. Mallada, J. Santamaría, Amine-functionalized mesoporous silica: a material capable of CO_2 adsorption and fast regeneration by microwave heating, AlChE J. 62 (2) (2016) 547–555, https://doi.org/10.1002/aic.15118.ISSN 00011541
[27] C. Ellison, J. Hoffman, D. Shekhawat, Comparison of microwave and conventional heating for CO_2 desorption from zeolite 13X, Int. J. Greenh. Gas Control 107 (February) (2021) 103311, https://doi.org/10.1016/j.ijggc.2021.103311.
[28] E. Meloni, M. Martino, P. Pullumbi, F. Brandani, V. Palma, Intensification of TSA processes using a microwave-assisted regeneration step, Chem. Eng. Process. 160 (October 2020) (2021) 108291, https://doi.org/10.1016/j.cep.2020.108291.
[29] C.J.E. Bajamundi, J. Koponen, V. Ruuskanen, J. Elfving, A. Kosonen, J. Kauppinen, J. Ahola, et al., Capturing CO_2 from air: technical performance and process control improvement, J. CO2 Util. 30 (December 2018) (2019) 232–239, https://doi.org/10.1016/j.jcou.2019.02.002.
[30] J. Elfving, J. Kauppinen, M. Jegoroff, V. Ruuskanen, L. Järvinen, T. Sainio, et al., Experimental comparison of regeneration methods for CO_2 concentration from air using amine-based adsorbent, Chem. Eng. J. 404 (July 2020) (2021) 126337, https://doi.org/10.1016/j.cej.2020.126337.
[31] M. Schellevis, T. van Schagen, W. Brilman, Process optimization of a fixed bed reactor system for direct air capture, SSRN Electron. J. (March) (2021), https://doi.org/10.2139/ssrn.3821508.
[32] Q. Yu, D.W.F. Brilman, Design strategy for CO_2 adsorption from ambient air using a supported amine based sorbent in a fixed bed reactor, Energy Procedia 114 (November 2016) (2017) 6102–6114, https://doi.org/10.1016/j.egypro.2017.03.1747.
[33] M.J. Bos, S. Pietersen, D.W.F. Brilman, Production of high purity CO_2 from air using solid amine sorbents, Chem. Eng. Sci. 2 (2019) 100020, https://doi.org/10.1016/j.cesx.2019.100020.
[34] W.R. Alesi, J.R. Kitchin, Evaluation of a primary amine-functionalized ion-exchange resin for CO_2 capture, Ind. Eng. Chem. Res. 51 (19) (2012) 6907–6915, https://doi.org/10.1021/ie300452c.
[35] R. Veneman, N. Frigka, W. Zhao, Z. Li, S. Kersten, W. Brilman, et al., Adsorption of H_2O and CO_2 on supported amine sorbents, Int. J. Greenh. Gas Control 41 (2015) 268–275, https://doi.org/10.1016/j.ijggc.2015.07.014.
[36] R.R. Meredith, Engineers' Handbook of Industrial Microwave Heating, IET, 1998.
[37] S. Lupi, Fundamentals of Electroheat, 2017. doi:10.1007/978-3-319-46015-4.
[38] D.C. Dube, Study of Landau–Lifshitz–Looyenga's formula for dielectric correlation between powder and bulk, J. Phys. D 3 (11) (1970) 313, https://doi.org/10.1088/0022-3727/3/11/313.
[39] Lanxess, Lewatit VP OC 1065 Technical Datasheet, 2017.
[40] R. Veneman, W. Zhao, Z. Li, N. Cai, D.W.F. Brilman, et al., Adsorption of CO_2 and H_2O on supported amine sorbents, Energy Procedia 63 (2014) 2336–2345, https://doi.org/10.1016/j.egypro.2014.11.254.
[41] M.B. Swami, P.G. Hudge, V.P. Pawar, Dielectric properties of benzylamine in 1,2,6-hexanetriol mixture using time domain reflectometry technique, J. Adv. Dielectr. 6 (4) (2016), https://doi.org/10.1142/S2010135X1650034X.